

Physically-Based Glare Effects for Digital Images

Greg Spencer*
Taligent, Inc.

Peter Shirley†
Cornell University

Kurt Zimmerman‡
Indiana University

Donald P. Greenberg§
Cornell University

Abstract

The physical mechanisms and physiological causes of glare in human vision are reviewed. These mechanisms are scattering in the cornea, lens, and retina, and diffraction in the coherent cell structures on the outer radial areas of the lens. This scattering and diffraction are responsible for the “bloom” and “flare lines” seen around very bright objects. The diffraction effects cause the “lenticular halo”. The quantitative models of these glare effects are reviewed, and an algorithm for using these models to add glare effects to digital images is presented. The resulting digital point-spread function is thus psychophysically based and can substantially increase the “perceived” dynamic range of computer simulations containing light sources. Finally, a perceptual test is presented that indicates these added glare effects increase the apparent brightness of light sources in digital images.

CR Categories and Subject Descriptors: I.3.0 [Computer Graphics]: General; I.3.6 [Computer Graphics]: Methodology and Techniques.

Additional Key Words and Phrases: bloom, flare, glare, lenticular halo, vision.

1 Introduction

There is a continual quest for photorealistic simulations, not only by accurately modeling the physical behavior of light reflection, propagation and transport, but by the creation of images that are “perceived” to be realistic. Unfortunately, a digital image can only be as realistic as the limited color gamut, dynamic range, spatial resolution, field-of-view, and stereo-capacity that the display medium will allow. If we had a display medium which could produce the high luminances of real scenes, we would calculate the radiometric quantities for each pixel in the two dimensional image lattice, and send the resulting lattice to the display. However, digital images are displayed on devices with from 256 to 1024 luminance levels and a maximum luminance of approximately 50 cd/m^2 .

To illustrate why this lack of intensity can hamper realism, consider the difference between the perception of a displayed



Figure 1: Carl Saltzmann, *Erste elektrische Straßenbeleuchtung in Berlin, Potsdamer Platz, 1884.*

digital image of a single white pixel on a black background, and the real experience of looking at a small incandescent bulb. The real bulb differs from the digital image in two important ways. The first difference is a qualitative “brightness” that the bulb possesses. The second difference is the hazy glow that can be seen around the bulb. This glow not only gives an impression of greater brightness, but it can also interfere with the visibility of objects near the bulb.

We can improve the realism of simulated images by adding effects which perceptually expand and enhance the perceived dynamic range. These effects are most pronounced where bright light sources are visible within the scene. Perceptual effects which exaggerate the brightness of objects in an image have long been used in artistic expression. The impressionists, in the late 19th century depicted the brightness of illuminating sources by adding tell-tale radial lines (Figure 1). Cinematographers often add etched lenses to create special effects around lights, starbursts, or explosions to make them appear brighter than otherwise. Although these techniques are not psychophysically accurate, each produces the desired impression by exaggerating the luminance of the sources.

The idea of adding glare effects to a digital image is not new. Nakamae et al. [20] pointed out that the limited dynamic range of CRTs prevents the display of luminaires at their actual luminance values, and that adding streaking and blooming around the luminaires helps give the appearance of glare. While Nakamae et al.’s glare algorithm is extremely effective in conveying an impression of luminaire intensity, it does not account for the visual masking effects of glare, which is needed for object-visibility prediction.

*10201 N. De Anza Blvd., Cupertino, CA 95014.

Greg.Spencer@Taligent.COM.

†580 ETC, Ithaca, NY 14850. shirley@graphics.cornell.edu.

‡Lindley Hall, Bloomington, IN 47405.

kuzimmer@cs.indiana.edu.

§580 ETC, Ithaca, NY 14850. dpg@graphics.cornell.edu.

Permission to make digital/hard copy of part or all of this work for personal or classroom use is granted without fee provided that copies are not made or distributed for profit or commercial advantage, the copyright notice, the title of the publication and its date appear, and notice is given that copying is by permission of ACM, Inc. To copy otherwise, to republish, to post on servers, or to redistribute to lists, requires prior specific permission and/or a fee.

©1995 ACM-0-89791-701-4/95/008...\$3.50

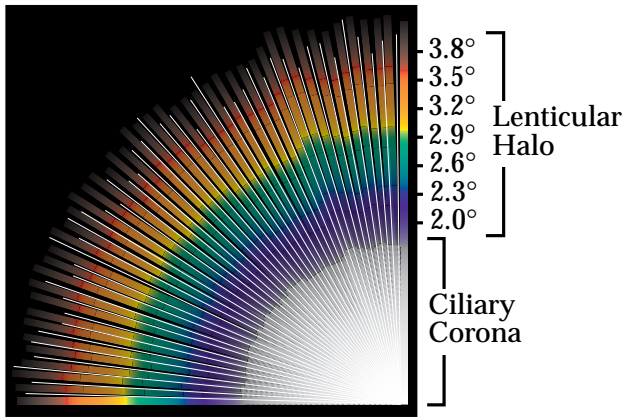


Figure 2: The ciliary corona and lenticular halo for a small white light source (after [29]).

Our approach has been to model the physical effects, primarily caused by the interaction of light rays and the physiology of the human eye. For many years, researchers in optics, psychophysics, and illumination engineering have attempted to determine the mechanisms behind glare, and to quantify the effects of glare on viewers. A camera lens filter that mimics the underlying mechanisms of glare in human vision has recently been developed, and had better results than conventional glare filters for some effects [1].

Glare effects can be subdivided into two major components: *flare* and *bloom*. Flare is composed of a *lenticular halo* and a *ciliary corona* (Figure 2), and is primarily caused by the lens [29]. Bloom is caused by scattering from three parts of the visual system: the cornea, lens and retina (Figure 3). The lenticular halo, ciliary corona, and bloom are the dominant contributing factors to glare effects and greatly affect our perception of the brightnesses of light sources.

Rays of the ciliary corona appear as radial streaks emanating from the center of the source. Similar ray patterns associated with other coronas have been studied by physicists and are caused by random fluctuations in refractive index of the ocular media [15].

The lenticular halo is observed as a set of colored, concentric rings, surrounding the light source and distal to the ciliary corona. The somewhat irregular rings are composed of radial segments, where the color of each segment of the ray varies with its distance from the source. The apparent size of the halo is constant and independent of the distance between the observer and the source. This phenomenon is caused by the radial fibers of the crystalline structure of the lens [29, 15].

Bloom, frequently referred to as “veiling luminance” is the “glow” around bright objects. Bloom causes a reduction in contrast that interferes with the visibility of nearby objects, such as the night-time view of the grill between two car headlamps. Bloom is caused by stray light attributed to scatter from three portions of the eye: the cornea, the crystalline lens, and the retina, all with approximately equal contributions [33].

The physiology of the eye and the resultant physical effects are explained in greater detail in the following section. In Section 3 we develop the quantitative aspects of this glare in terms of the *point-spread function* of the human eye and present an algorithm for generating the digital flare filter that approximates the point spread function. In Section 4 we describe a brief perceptual experiment which verified

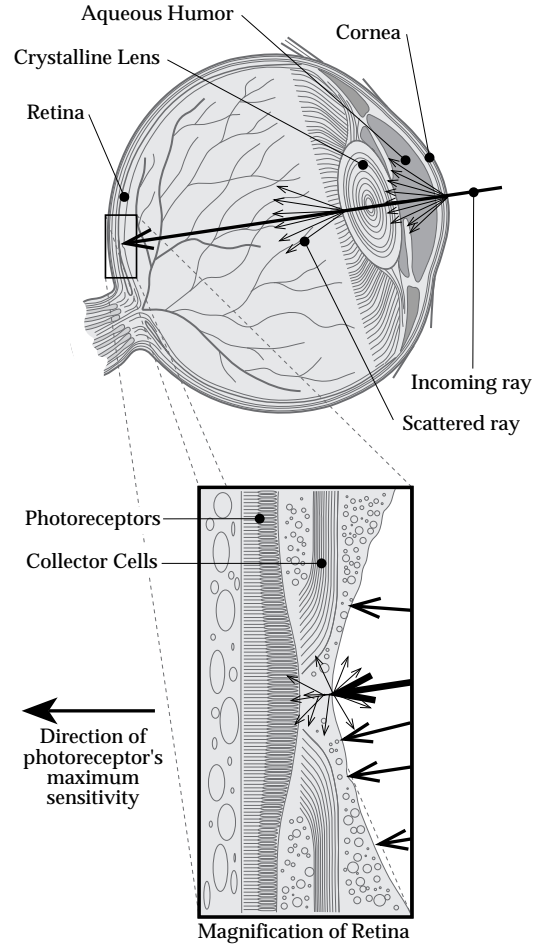


Figure 3: Scattering in the eye (after [28]). A small beam of light entering the eye is partially scattered in the cornea, the lens, and in the first layer of the retina.

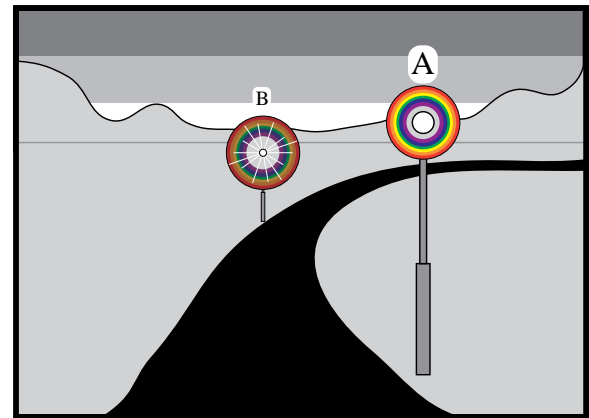


Figure 4: Glare around a nearby source **A** and distant source **B**. Since the halo subtends the same angle for each source, the halo around **B** has the illusion of being larger than the halo around **A**.

the increase in perceived brightness. We conclude the paper showing several vivid examples and recommendations for future work.

2 Physiology and Physical Effects

The physical mechanisms behind glare have been studied since the late 19th century [29] and have been a matter of debate until quite recently [15]. In this section we present the physical origins of glare, drawing mainly on Simpson's work on lenticular haloes [29], and Vos [33] and Hemenger's [15] work on scattering in the eye.

2.1 Lenticular Halo

When one observes a point source of light in a dark surround, there appears to be a series of concentric colored rings around the source. This is known as the lenticular halo (Figure 2). No matter how far away the source is from the observer, the haloes always subtend the same angle at the eye. As shown in Figure 4, this creates an illusion that haloes around distant light sources appear larger than haloes around nearby sources. The intensity of the halo decreases with distance, and streaks are seen if the source subtends a sufficiently small solid angle.

The lenticular halo is caused by the circular optical grating formed by the radial fibers at the periphery of the crystalline lens. This was first explained by Druault in 1897 [29], and experimentally verified by the Emsley-Fincham tests in 1922 [29]. A clear explanation, first presented by Simpson in 1953 is illustrated below.

Figure 5(a) shows a biconvex lens with a circular grating etched into the outer portion of the lens. The axis of the lens is through the center, perpendicular to the plane of the paper, and meets the focal plane at point F . If we consider a small segment of the circular grating at G , where the lines of the segment are nearly parallel, we have a typical parallel diffraction grating.

Light is refracted according to the following equation:

$$\sin \theta = \frac{\lambda}{e},$$

where θ is the angular deviation of the light path, λ is the wavelength, and e is the distance between adjacent grating spaces. Thus, when white light is passed through the region G , and focused on the focal plane, the violet components appear at V , F , and V' , and the red components appear at R , F , and R' . Thus two lines are formed, each one radiating outward and containing the full range of spectral colors. As we circumferentially traverse the circular grating, two overlapping haloes are produced.

The biconvex lens with the circular optical grating is actually a simplified model of the crystalline lens of the human eye (Figure 5(b)). This is composed of fibers which are relatively large strips of transparent material having a cross-section of roughly hexagonal shape [10]. Although the central part of the lens is optically homogeneous, the exterior portions act as an optical grating with a spacing of e , the width of the fibers.

A beam of light which is less than 3mm in diameter can pass through the clear portion of the lens, but subtending larger angles will always pass through the grating, thus creating the lenticular halo. This means that haloes are not seen in daylight levels of illumination (when the pupil is 2mm across) but is seen in darker conditions.

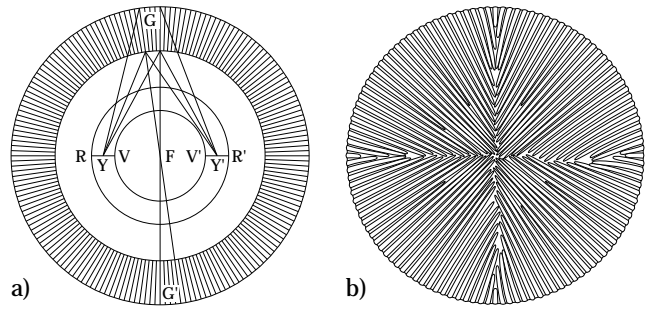


Figure 5: a) Diagram of the etched biconvex lens (after [29]). b) Cell structure of the Crystalline Lens (cell size exaggerated).

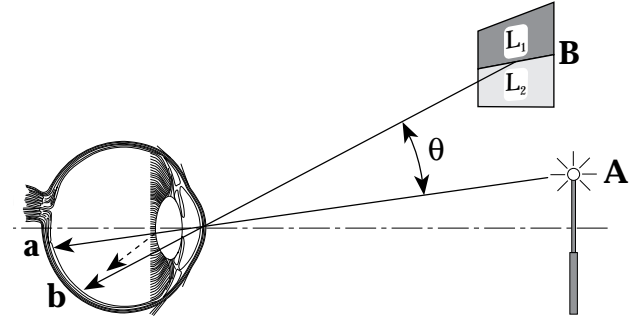


Figure 6: A reduction in contrast that results from scattered light in the eye causes a reduction in contrast that depends on θ , the angle of separation.

2.2 The Ciliary Corona

The ciliary corona is depicted in Figure 2 and consists of rays emanating from a point light source. These radial rays may extend beyond the lenticular halo, and are brighter and more pronounced as the angle subtended by the source decreases (Figure 4). The ciliary corona is caused by semi-random density fluctuation in the nucleus of the lens which causes forward scattering that is independent of wavelength [15]. As the size of the source increases, it appears that the ciliary corona blurs and contributes to the bloom effect. This is because superimposing the fine flare lines coming from each part of an areal source eliminates the crisp pattern of any given set of radial flare lines. Simpson observed that sources much larger than 20 minutes of arc did not have significant flare lines.

2.3 Bloom

Bloom, frequently referred to as “disability glare” or “veiling luminance” is best illustrated by the reduced visibility which occurs in the presence of bright light sources. This effect is attributed to the scattering of light in the ocular media, where the scatter contributions from the cornea, crystalline lens, and retina occur in roughly equal portions.

This effect is illustrated in Figure 6 where light from source A scatters inside the eye and is added to light coming from object B . This scattered light adds an effective luminance s that does not originate at B . Because light is added to both the light and dark parts of object B , the contrast ratio L_2/L_1 is reduced. In addition, since sensitivity to absolute luminance difference decreases as the base luminance increases, the difference between L_1 and L_2 might be dis-

cernible, while the difference between $s + L_1$ and $s + L_2$ is not. The magnitude of s depends on the angle of separation θ , and the luminance and solid angle of the source. The quantitative details of this dependence will be discussed in Section 3.

Veiling luminance has been the subject of investigations for almost two centuries, and there is still some controversy surrounding some of the details of the mechanisms for glare. It is evident that the stray or scattered light plays a dominant role [15], but neural inhibitory effects may also be present at very small angles of incidence [33].

It is not feasible to document the large number of psychophysical studies performed on this subject, and the reader is referred to the annotated bibliography of Ronci and Stefanacci [24], as well as the more recent studies of Owsley et al. [22], Ross et al. [25], and Ijspeert et al. [17]. Investigations by Stiles [31], Cornsweet and Teller [9], Blackwell and Blackwell [3], Hemenger [15] and others all corroborate that the masking effect of glare is caused primarily by stray light. Direct evidence has also been obtained by observing the interior of the eye, revealing that the light scattering comes primarily from the cornea, crystalline lens, and retina (Figure 2). These cellular structures, many microns in diameter, scatter light independent of wavelength, much like a rough reflecting surface.

For the cornea and the lens, the light is scattered in a narrow forward cone with approximately a Gaussian distribution [5]. The corneal scattering can be differentiated from the lenticular scattering since it casts a shadow of the iris on the retina. The retina to retina scattering, although physically in all directions is only important in the same forward directions due to the drastically reduced directional sensitivity of the cone system to obliquely incident light (the ‘‘Crawford-Stiles’’ effect). Because the rod sensitivity does not have as high a directional sensitivity as the cones, the magnitude of glare is greater in dark (scotopic) conditions.

For these reasons, the light scattering is somewhat like a ‘‘blurring’’ or ‘‘blooming’’ effect with a sharp drop-off, and can be approximated with empirical formulae to match the experimental results.

3 Algorithm

Although at a high level we understand the physical mechanisms behind scattering in the eye, the exact structure of the cells in the eye is not known to the extent that we can simulate the scattering from first principles. In fact, current knowledge about the cell structure in the eye comes from inversion of observed scattering behavior [2, 15]. For this reason, we use psychophysical and phenomenological results in addition to physical modeling.

If the eye is focused on a ‘‘point source’’, then ideally a small discrete area of non-zero irradiance would fall on the retina. Because the eye is a real optical system, there will be some blurring of this signal on the retina. This blurring can be described by a ‘‘point source function’’ (PSF) for the eye. In Section 3.1 we describe quantitative glare models in terms of the PSF of the eye, and in Section 3.2 we show how this model can be simulated by convolving a radiometric image with a particular digital filter kernel.

3.1 Quantitative Model of Glare

There is approximate agreement on the exact perceptual contribution of the bloom for a ‘‘normal’’ viewer. Several researchers [16, 31, 11] have studied the magnitude of the

glare effect by examining the threshold of visibility of an object near a source that produces illuminance E_0 at the front of the eye. By turning the source off, and adding a background luminance L_v that makes the object barely visible, the ‘‘equivalent veiling luminance’’ L_v can be found. This has led to empirical equations taking the general form:

$$L_v(\theta) = \frac{kE_0}{f(\theta)}, \quad (1)$$

where L_v is the equivalent veiling luminance in cd/m^2 , E_0 is the illuminance from the glare source at the eye in lx , k is a constant depending on the experimental conditions, θ is the angle between the primary object and the glare source in degrees, and f is an experimentally determined function. Various values for k between 3 and 50 have been used, and $f(\theta)$ is usually set to be θ^N or $(\theta + \theta_0)^N$ with N ranging from 1.5 to 3. Since the bloom is viewer-dependent, all of these values for k and f can be considered to be in some sense reasonable, but recently an approximate consensus has been reached on the details of these parameters.

The form of Equation 1 is somewhat confusing because it involves both luminance and illuminance. Vos has presented the equation in a less intimidating form by rewriting it as a *point spread function* (PSF). A PSF is a density (unit volume) function defined on the visual field that describes how a unit volume point source (a delta function) is ‘‘spread’’ onto other points of the visual field. If we assume that the unscattered component of Equation 1 is unchanged (appears as an exact point source), then the PSF $P(\theta)$ is:

$$P(\theta) = a\delta(\theta) + \frac{k}{f(\theta)}, \quad (2)$$

where $\delta(\theta)$ is an ‘‘ideal’’ PSF and a is the fraction of light that is not scattered.

The form of Equation 2 assumes that there is no energy loss in the system. This is not the case, and has been the cause of some debate in the glare literature. The perceived fraction of light scattered in Equation 2 (i.e. $\int k/f(\theta)$) is roughly 10% for normal viewers. However, physical experiments suggest that as much as 40% of the light is actually scattered [26, 4]. Researchers have investigated this apparent contradiction. The most common explanation is that angular dependence of the sensitivity of the cones in the retina (the Crawford-Stiles effect [36]) effectively absorbs some of the stray light, particularly for θ more than a few degrees. This same effect causes light transmitted by the outer edge of a fully dilated pupil to be 5-10 times less effective than light through the center of the pupil [33]. This implies that we should trust the ten percent figure for our purposes because it is the perceptual quality of the light that we need to account for. Thus, we should realize that Equation 2 represents a normalized perceptual PSF and does not measure the spread of retinal illuminance.

Recently, Vos has attempted to unify the large number of PSF models for the eye [33]. In this section we review Vos’ work, and add two effects studied by Hemenger [15] not accounted for in Vos’ model.

If the point spread function is defined on the hemisphere of directions entering the eye, where α is the angle from the gaze direction and ϕ is the angle around the gaze direction, then

$$\int_0^{2\pi} \int_0^{\frac{\pi}{2}} P(\theta) \sin \theta d\theta d\phi = 1, \quad (3)$$

where the angles are measured in radians. This normalization condition asserts that the PSF P redistributes energy,

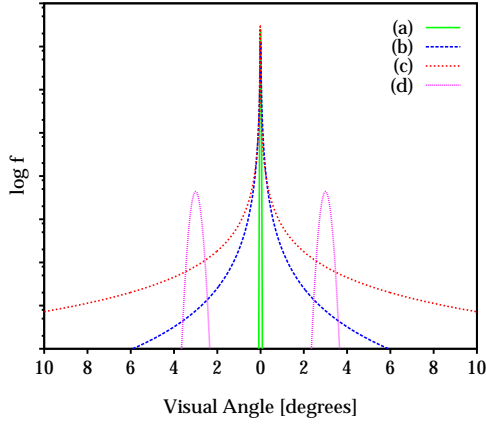


Figure 7: The PSF components (a) f_0 , (b) f_1 , (c) f_2 , and (d) f_3 .

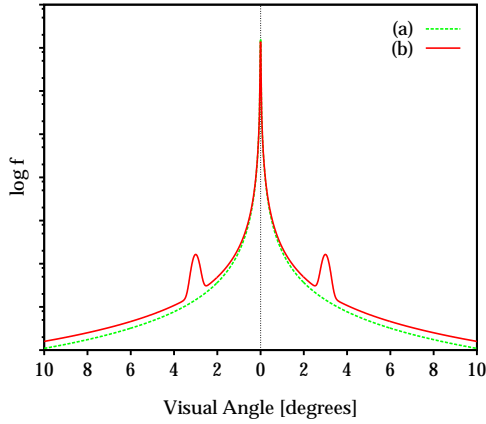


Figure 8: (a) The photopic PSF P_p . (b) The scotopic PSF P_s .

but does not emit or absorb energy. If the optical system does absorb energy, this is accounted for by a constant separate from the PSF.

Because the glare literature reports its results in degrees, we can rewrite the PSF normalization condition for a $P(\theta)$, where θ is in degrees:

$$\frac{\pi^2}{90} \int_0^{90^\circ} P(\theta) \sin \theta d\theta = 1. \quad (4)$$

Any non-negative function of θ that satisfies Equation 4 is a candidate for a point spread function. This means that any weighted average of functions that each satisfy Equation 4 is also a candidate. Vos [33] has reviewed the various models for glare and noted that there are three different empirical components in the PSF for an eye. The first is a narrow Gaussian that represents the unscattered component. The second is a function that is roughly proportional to θ^{-3} that is dominant for non-zero θ less than one or two degrees. The third is a term proportional to θ^{-2} for θ more than a degree. Because both the θ^{-3} and θ^{-2} terms would blow up near $\theta = 0$, Vos replaces them with $(\theta + a)^{-2}$ and $(\theta + a)^{-3}$ for some empirical constant a , and suggests the following three normalized components:

$$f_0(\theta) = 2.61 \times 10^6 e^{-\left(\frac{\theta}{0.02}\right)^2},$$

for the central Gaussian,

$$f_1(\theta) = \frac{20.91}{(\theta + 0.02)^3},$$

for the θ^{-3} component, and

$$f_2(\theta) = \frac{72.37}{(\theta + 0.02)^2},$$

for the θ^{-2} component. These functions are shown in Figure 7. The function f_0 represents the unscattered component of the light. It shows the typical Gaussian shape expected for an real-world imaging system. This term should vary slightly with pupil size [5] but for our purposes could be replaced by a delta function because the angular size of the Gaussian will be much smaller than a pixel width.

Finally, Vos suggests the following combination for the PSF of a normal viewer:

$$P_p(\theta) = 0.384f_0(\theta) + 0.478f_1(\theta) + 0.138f_2(\theta). \quad (5)$$

This PSF is subscripted with a “p” because it is appropriate for observers in a *photopic* (light adapted) state. The light adaptation of a viewer is described by one of three basic states [23]: less than 0.01 cd/m^2 is the *scotopic region* (night vision); the range $0.01\text{--}3 \text{ cd/m}^2$ is the *mesopic region* (mixed night and day vision); more than 3 cd/m^2 is the *photopic region* (day vision). The graph of Equation 5 is shown in Figure 8.

3.1.1 Adding the lenticular halo

For pupil diameters less than three millimeters, Simpson reports that the coherent fibers in the lens are blocked by the iris. The pupil diameter is influenced by many factors such as age, mood, and the spectral distribution of incoming light, but it is primarily related to the field luminance of the scene. Moon and Spencer (1944) [36] relate average pupil diameter D (in mm) to field luminance L (in cd/m^2):

$$D = 4.9 - 3 \tanh(0.4(\log_{10} L + 1)).$$

This yields a pupil diameter of about 3 mm for $L = 10 \text{ cd/m}^2$, which is the field luminance of a dimly lit interior. We should expect no lenticular halo in daylight conditions, a mild lenticular halo in dimly lit rooms, and prominent lenticular haloes for dark scenes.

It was observed by Mallero and Palmer [18] that light at 568 nm caused a lenticular halo of approximately 3° radius with an angular width of 0.35° . Based on this observation, Hemenger [15] used the following empirical formula to model the lenticular halo with these properties produced by light at 568 nm :

$$C(t) = B e^{-19.75(\theta - \theta_0)^2}, \quad (6)$$

where B is a constant and $\theta_0 = 3^\circ$.

Since the angle of a diffraction pattern peak is proportional to wavelength, we can establish the formula:

$$\theta_0(\lambda) = \frac{\lambda}{568}.$$

Since we expect the same fraction of incident energy to be diffracted for each wavelength, we can construct a unit volume PSF for the lenticular halo:

$$f_3(\theta, \lambda) = 436.9 \frac{568}{\lambda} e^{-(\theta - 3 \frac{\lambda}{568})^2}. \quad (7)$$

Mallero and Palmer also observed that in dark conditions the halo at 568nm had about ten times the luminance of the ciliary corona. From this fact, and from Equation 5 and Equation 7 we see that $P_p(3^\circ) = 1.462$ and $f_3(3^\circ, 568) = 436.9$, so a reasonable coefficient for f_3 will make the ring appear ten times as bright as P_p , so the coefficient we use is $10 \times 1.462/436.9 = 0.033$. However, this assumes a fully dilated pupil, which is only true for scotopic conditions. So we assume that about half of the radial fibers of the lens are exposed, calling for a coefficient for f_3 of 0.016, resulting in the equation:

$$\begin{aligned} P_m(\theta, \lambda) = & 0.368f_0(\theta) + \\ & 0.478f_1(\theta) + \\ & 0.138f_2(\theta) + \\ & 0.016f_3(\theta, \lambda). \end{aligned} \quad (8)$$

This assumes the lenticular halo is diverted from the central peak. The subscript m refers to a *mesopic* observer, whose pupil is large, but whose cones are still active.

For darker conditions the amount of glare may be higher. At 0.15 cd/m^2 there is 50% more straylight than at 100 cd/m^2 [22]. This suggests an alternative form for the darkest point-spread function:

$$\begin{aligned} P_s(\theta, \lambda) = & 0.282f_0(\theta) + \\ & 0.478f_1(\theta) + \\ & 0.207f_2(\theta) + \\ & 0.033f_3(\theta, \lambda). \end{aligned} \quad (9)$$

The graph of P_s is shown in Figure 8.

3.1.2 Viewer-Specific Variation in PSF

There is an increase in glare with age, although the shape of the PSF stays the same [13]. If there are no cataracts, Vos [33] has established a rough age relation:

$$\begin{aligned} P_p(\theta) = & (0.384 - 6.9 \times 10^{-9}A^4)f_0(\theta) + \\ & 0.478f_1(\theta) + \\ & (0.138 + 6.9 \times 10^{-9}A^4)f_2(\theta), \end{aligned} \quad (10)$$

where A is the age of the viewer in years. This change in vision is caused primarily by optical changes in the eye [12], but there is some loss due to neural changes as well [21]. Equation 10 implies that the fraction of light scattered more than 0.05° increases from 0.36 at age 20 to 0.45 at age 60. The ratio of this light to unscattered light approximately doubles between the ages of 20 and 70. The situation can be even worse for viewers with cataracts, where the fraction of light that is scattered can be close to one [14]. There are no sex differences in the PSF [22], and only minor differences for viewers with different pigmentation [17]. The formulas for P_m and P_s will have similar behavior to P_p , but the coefficient for f_3 may remain relatively constant because the pupil diameter becomes more static with age. This may result in mild lenticular haloes in photopic conditions for old viewers.

There is also an age-related color shift toward the yellow in the light transmitted by the lens. This, as well as increased fluorescence of the lens, can cause an additional reduction in visibility for elderly viewers in some viewing conditions such as twilight [6] and scotopic conditions [21]. The yellowing of the lens also causes metamerism to vary with age [8]. Since age-related changes vary widely from viewer to viewer, these

studies are primarily useful for establishing guidelines for the design of environments that are safe for “typical” elderly viewers.

3.2 Digital Glare Filter Generation

The glare formulae of Section 3.1 can be applied directly to digital images by using a digital point spread function to spread energy in high-intensity pixels to nearby pixels. This basic strategy has been used by Nakamae et al. [20] and Chiu et al. [7]. Unlike these previous approaches, we use different flare filters based on the adaptation state of the viewer.

To develop a filter for a particular image, we first construct digital versions of $f_0(\theta)$, $f_1(\theta)$, $f_2(\theta)$, and $f_3(\theta)$. Since each of these filters must have unit volume, we can calculate each filter proportional to a given function, and then renormalize the filter so that all pixels sum to one. These filters and the images they are applied to are stored in Ward’s floating point file format [35], so that the small values in the off-center filter pixels are not lost. We compute the filter for an $N \times N$ image, where $N = 2n + 1$ so there is guaranteed to be a single central pixel. We number these pixels $(0, 0)$ through $(N - 1, N - 1)$ and we calculate the angle $\Delta\theta$ subtended by the pixels of the image that we will add glare to. This assumes a relatively small field of view so that $\Delta\theta$ can be approximated by a constant for all pixels. To calculate the value $d(i, j)$ for a particular flare component $f(\theta)$ we evaluate the integral

$$p(i, j) = \int_{i-0.5}^{i+0.5} \int_{j-0.5}^{j+0.5} f \left(\Delta\theta \sqrt{(u-n)^2 + (v-n)^2} \right) dv du.$$

We use the trapezoidal rule to evaluate this integral. For f_0 , f_1 , and f_2 we use 10000 sample points in the central part of the filter where there is rapid change in the function, and 100 sample points elsewhere. To construct the colors in the lenticular halo, $f_3(\theta, \lambda)$, we process Equation 7 for 50 wavelengths from 400 nm to 700 nm and then convert to a trichromatic transform as described by Meyer [19]. This halo is not a classic “pure” spectrum because each wavelength bleeds into its neighbors, so it is not on the boundary of the visible part of the CIE diagram and is thus easier to display on a monitor gamut. The resulting pattern is shown in Figure 9 and is consistent with Simpson’s observations (Figure 2).

Unfortunately, the filters calculated in this manner will lack the flare lines we expect (Figure 2), because they are spatial averages over areas that cover many flare lines. We need to add these flare lines without disturbing the macroscopic structure suggested by Equations 5, 8, and 9. We add flare detail to our digital filter by drawing random antialiased radial lines of random intensity in the range $[0, 1]$ on a digital image the same size as our filter. We draw a number of lines to visually match Simpson’s observations (Figure 2). We assume that the ciliary corona (represented by $f_1(\theta)$ and $f_2(\theta)$) is composed of one set of flare lines, and that the lenticular halo (represented by $f_3(\theta)$) is composed of a different set of flare lines. This separation is consistent with the fact that there is a different physical mechanism for the two components, as was discussed in Section 2.

We take the random pattern of flare lines and adjust it so that it has an average pixel value of 1.0, and that each small neighborhood also has an average value of 1.0. This has the effect of increasing the pixel intensity radially because the fraction of pixels in a streak decreases radially from the

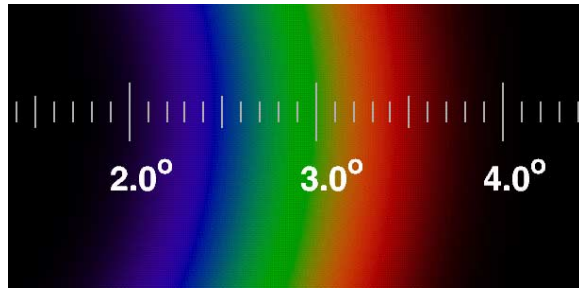


Figure 9: Algorithmically generated lenticular halo. Compare to Simpson's observed values in Figure 2.

center. This new pattern is then multiplied by the original flare functions, which gives them the appropriate detail without changing their carefully calculated macroscopic behavior. This process is shown in Figure 10, for the particular case of $P_m(\theta)$ (Equation 8), where the filter is built up in stages.

The filter is independent of a particular image, but must be recomputed for a new field-of-view because the angular size of a pixel changes. Thus only one filter is computed for an animation sequence that uses one set of camera parameters. The width and height of the filter is double the width and height of the target image. Because the values in the filter decrease away from the center (except for the lenticular halo which is approximately a factor of ten larger than its nearby interior neighbors), we can use only a central portion of the filter when processing dim pixels. This enormously decreases the execution time (approximately a factor of 100 in our implementation on the images in Section 5). Because the viewer will experience *actual* glare for the displayed pixels, we only need add glare to pixels whose full intensity is not displayed. So if the maximum displayable intensity is I_m , and the computed intensity for a given pixel is I , where $I > I_m$, the filter is applied to the value $I - I_m$. Note that the filter is applied at each of these bright pixels in the source image, which is spread to the appropriate regions of the destination image.

4 Perceptual Tests

Once the techniques are developed to simulate flare and bloom, simple experiments can be conducted to determine the perceptual effects.

In one simple experiment, two stimuli, one with a ciliary corona, and one without, were compared to see which one was perceived to be brighter. Each greyscale image was presented in a window with a short presentation time, 400ms or 700ms. Colormap manipulation was implemented to control the presentation time to within $\pm 10ms$. Each image window was 300 by 300 pixels on the 1280 by 1024 display monitor. The presentation window was the only item visible on a screen with a black background.

The basic "staircase" method was utilized in the experiment with a three-way forced choice (choices were "Image A Brighter", "Image B Brighter" and "Neither Image Brighter"). The staircase method refers to a method of decreasing the adjustment to a stimulus to converge on a threshold while virtually eliminating predictive bias [36]. Images were presented on a Sony Trinitron 19 inch display connected to a Hewlett-Packard 9000/750 with a VGRX Graphics card.

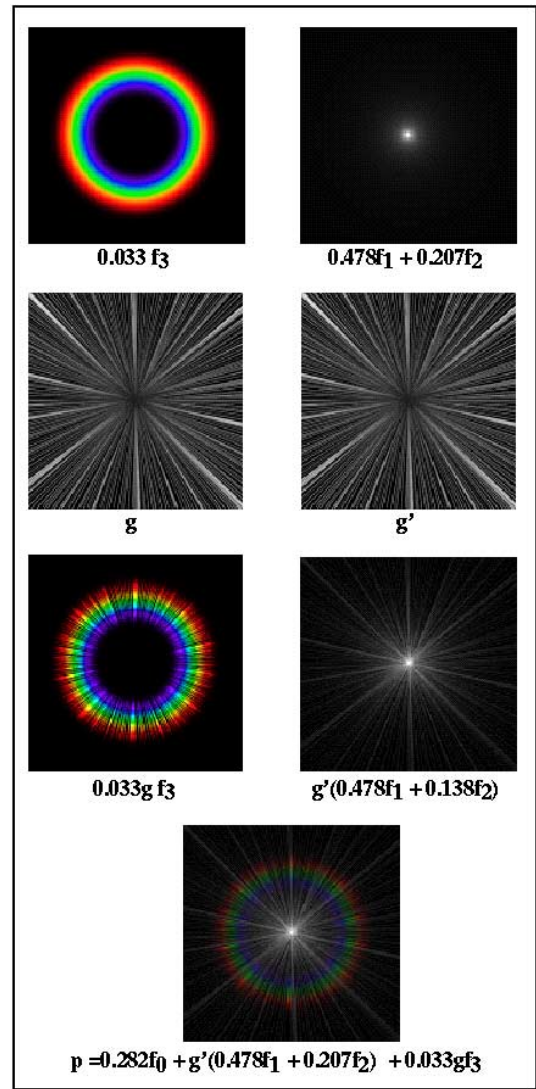


Figure 10: Overview of the construction of the scotopic point-spread filter P_s .

One window contained an image with the ciliary corona flare filter applied, and the other contained an identical image, except that the light source was replaced with a hardware-drawn disc surrounded by an annulus of one-third the intensity of the central disc (Figure 11(a)). The maximum intensity of the source with the corona flare was 75% of the maximum value displayable by the display device. The intensity of the disc varied from 0 to 100% of the maximum value.

Trials were arranged into two groups, with and without context for the source. In one group, the light source was presented by itself, in the center of a black field (Figure 11(b)). In the other group, the light source was placed into the context of a light bulb at the end of a desk lamp on a desk (Figure 11(c)). The order in which these groups of trials was run was randomized – half of the subjects performed the experiment with the context set first, and the other half observed the context free environments first. The glare images were also randomly swapped with the disc images so that one type of image did not always appear in the

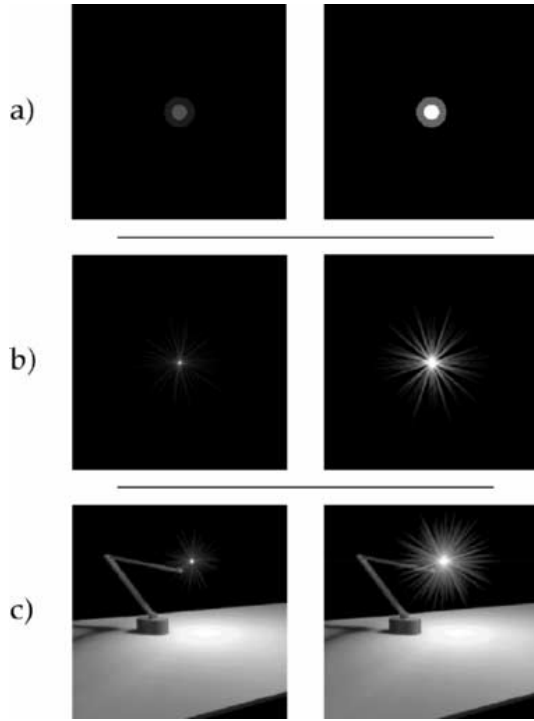


Figure 11: Sample stimuli showing the lowest and highest flare intensity.

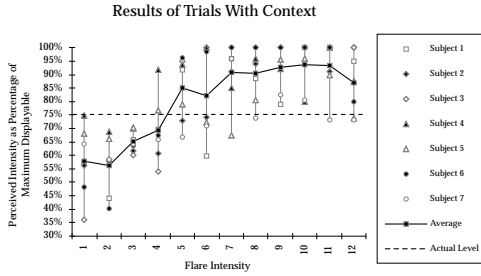


Figure 12: Stimulus with context.

same side of the display. In both groups of trials, there were 12 glare images, ranging from a simple slightly blurry dot to a light source which had too much glare to be believable. The entire experiment took place in a darkened room, so that the intensity of the test images would appear brighter overall, and enhance the glare effect.

4.1 Experimental Results

The experiment was conducted with a group of seven subjects, generating a statistically significant sample, given the small deviation usually present in brightness perception experiments.

The results, shown in Figures 12, and 13, show the expected response to the glare increase. If the glare had no effect, then the perceived intensity would be constant, as shown by the horizontal line at the 75% level.

The presence of a context (a lamp on a table) had no significant influence on the user's perception, but subjects did report having more confidence about the absolute brightness of the light source when the context was present.

Comparison of With and Without Context



Figure 13: Overall results of experiment.

The results indicate a fairly strong effect due to glare. This observation implies that applying a glare filter improves the apparent dynamic range of an image.

5 Examples

The digital filters of Section 4 were applied to several digital images. By contracting the filter radius for dim pixels, we were able to run the filters in approximately one to three minutes per image on a HP9000/755. All of the images are shown before and after application of the flare filter.

The scotopic PSF P_s was applied to a night scene (Figure 14). Note that the haloes stay the same size for sources at different distances. The cars in two filtered images are at different angles, so only the car on the bottom shows appreciable glare. Also notice that the brightness of the headlights at different angles can only be detected once the glare is added. The images in Figure 14 we desaturated so that the saturation in HSV space was reduced by 70% to simulate scotopic (rod) vision. The image was not completely desaturated because color vision degrades gradually and is still partially active even under moonlight (about 0.03 cd/m^2) [30].

Figure 15 shows an application of the mesopic PSF P_m to a rendered image. Note that the lenticular halo is prominent.

Figure 16 shows an application of the photopic PSF P_p to a digital photo of a tree composited over a sky with luminance $4.0 \times 10^3 \text{ cd/m}^2$ and a sun disk of $7.5 \times 10^8 \text{ cd/m}^2$. The sun pokes through just a few holes in the leaves of the tree. Note that, as expected when viewing a bright scene, the lenticular halo is missing from Figure 16.

All of these images have some burn-out, where the value of the pixel goes above one. Ultimately, a more sophisticated tone mapping algorithm should be used [32, 7, 34, 27], so that the images will have the appropriate degree of object visibility, and qualitative lightness or darkness. This issue is not addressed in this work.

6 Conclusion

We have presented the mechanisms of glare in the human visual system, and have provided quantitative formulae used by the vision community that describe its magnitude. These mechanisms are scattering in the cornea, lens, and retina, and diffraction in the coherent cell structures on the outer radial areas of the lens. The scattering and diffraction are responsible for the "bloom" and "flare" lines seen around

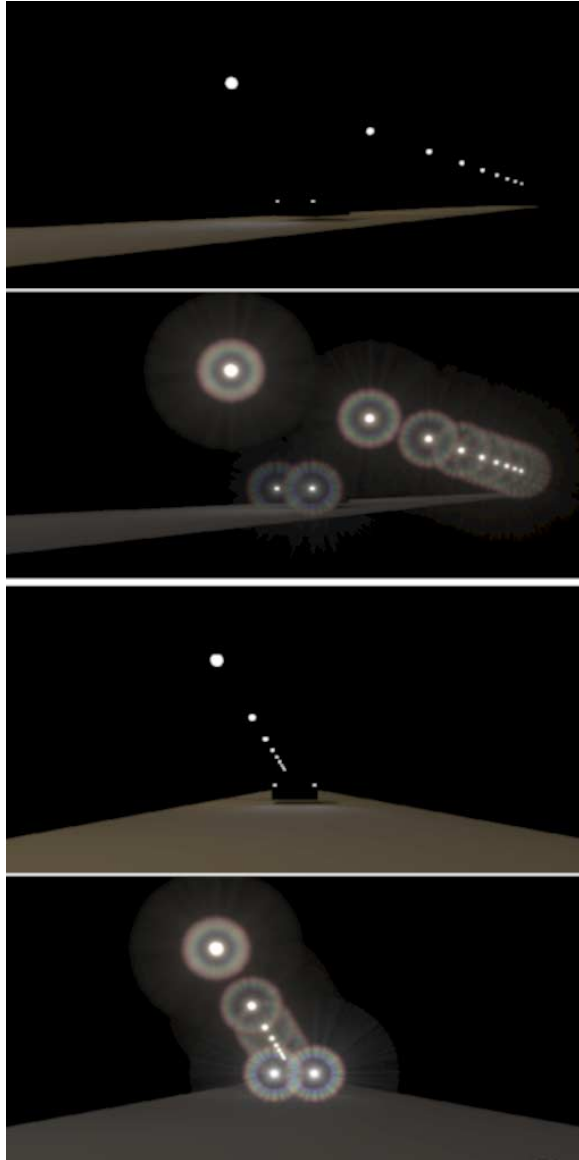


Figure 14: Two highway scenes before and after the scotopic glare algorithm. The orientation of the headlights is made obvious by the degree of glare.

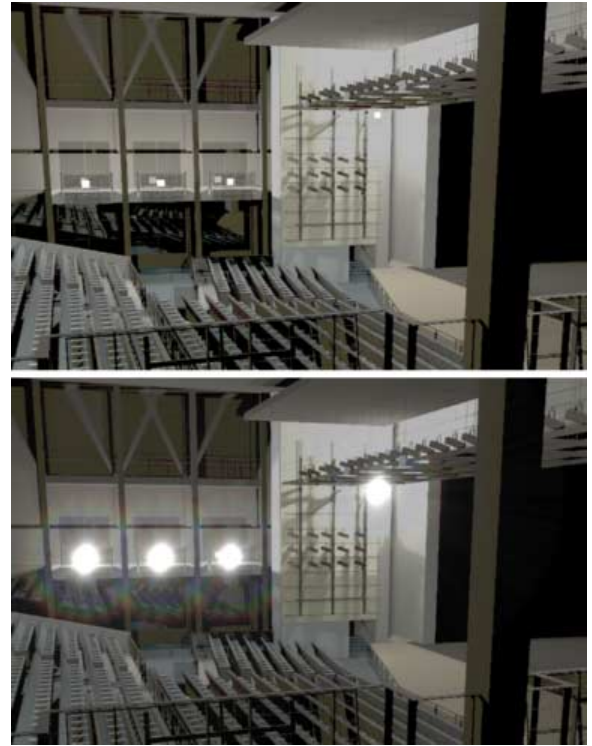


Figure 15: An indoor simulation before and after the mesopic glare algorithm..

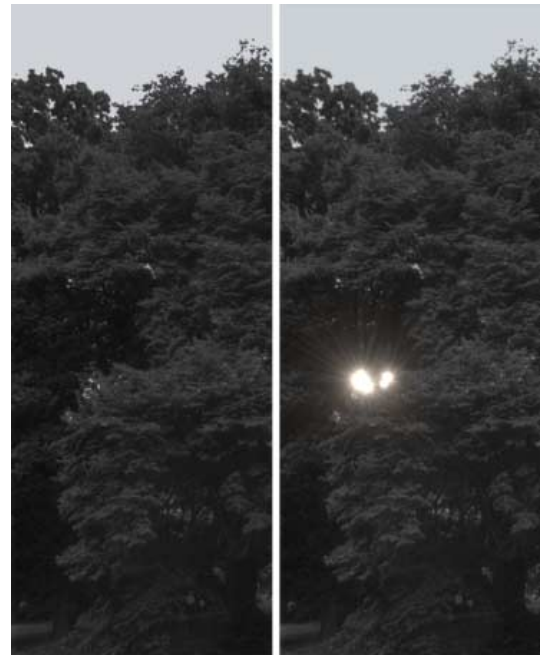


Figure 16: The Sun showing through leaves before and after the photopic glare algorithm. The location of the Sun is obvious only after the glare is added. Note that there is no lenticular halo because the pupil of the viewer is contracted.

very bright objects. The diffraction effects are responsible for the “lenticular halo”.

We have used these glare formulae to develop a digital point-spread function to add glare effects to digital images, and have run a perceptual experiment that indicates that the added glare increases the effective dynamic range in a digital image. Because the physically-based glare effects are expensive to compute, future work should focus on developing efficient methods that yield the same perceptual effects as the physically-based glare.

Acknowledgements

Thanks to Dan Kartch for help with the content and format of the paper, Andrew Kunz for help on image of the tree, Brian Smits for providing the theater image, Ben Trumbore and Bruce Walter for detailed comments on the paper, Alireza Esmailpour and Georgios Sakas for help obtaining a good reproduction of the Saltzman painting, to Ken Torrance for proving important pointers into the optics literature, and to Jim Ferwerda for help understanding the methodology of psychophysics. This work was supported by the NSF/ARPA Science and Technology Center for Computer Graphics and Scientific Visualization (ASC-8920219) and by NSF CCR-9401961 and performed on workstations generously provided by the Hewlett-Packard Corporation.

References

- [1] BECKMAN, C., NILSSON, O., AND PAULSSON, L.-E. Intraocular scattering in vision, artistic painting, and photography. *Applied Optics* 33, 21 (1994), 4749–4753.
- [2] BETTELHEIM, F. A., AND PAUNOVIC, M. Light scattering of normal human lens 1. *Biophysical Journal* 26, 3 (April 1979), 85–99.
- [3] BLACKWELL, O. M., AND BLACKWELL, H. R. Individual responses to lighting parameters for a population of 235 observers of varying ages. *Journal of the IES* 2 (July 1980), 205–232.
- [4] BOETTNER, E., AND WOLTER, J. Transmission of the ocular media. *Investigative Ophthalmology* 1 (1962), 776.
- [5] CAMPBELL, F., AND GUBISCH, R. Optical quality of the human eye. *Journal of Physiology* 186 (1966), 558–578.
- [6] CARTER, J. H. The effects of aging on selected visual functions: Color vision, glare sensitivity, field of vision, and accommodation. In *Aging and Human Visual Function*, R. Sekular, D. Kline, and K. Dismukes, Eds., vol. 2 of *Modern Aging Research*. Alan R. Liss, Inc., 1982, pp. 121–130.
- [7] CHIU, K., HERF, M., SHIRLEY, P., SWAMY, S., WANG, C., AND ZIMMERMAN, K. Spatially nonuniform scaling functions for high contrast images. In *Graphics Interface '93* (May 1993), pp. 245–244.
- [8] COREN, S., AND GIRGUS, J. Density of human lens pigmentation in vivo measures over an extended age range. *Vision Research* 12, 2 (1972), 343–346.
- [9] CORNSWEET, T. N., AND TELLER, D. Y. Relation of increment thresholds to brightness and luminance. *Journal of the Optical Society of America* 55 (1975), 1303–1308.
- [10] DAVSON, H., Ed. *The Eye*, third ed., vol. 1a. Academic Press, inc. Ltd., London, 1984.
- [11] FRY, G. A re-evaluation of the scattering theory of glare. *Illuminating Engineering* 49, 2 (1954), 98–102.
- [12] HEMENGER, R. P. Intraocular light scatter in normal vision loss with age. *Applied Optics* 23, 12 (1984), 1972–1974.
- [13] HEMENGER, R. P. Small-angle intraocular light scatter: a hypothesis concerning its source. *Journal of the Optical Society of America A* 5, 4 (1987), 577–582.
- [14] HEMENGER, R. P. Light scatter in cataractous lenses. *Ophthalmological Physiological Optics* 10 (October 1990), 394–397.
- [15] HEMENGER, R. P. Sources of intraocular light scatter from inversion of an empirical glare function. *Applied Optics* 31, 19 (1992), 3687–3693.
- [16] HOLLADAY, L. Action of a light source in the field of view on lowering visibility. *Journal of the Optical Society of America* 14, 1 (1927), 1–15.
- [17] IJSPEERT, J. K., DE WAARD, P. W. T., VAN DEN BERG, T., AND DE JONG, P. The intraocular straylight function in 129 healthy volunteers; dependence on angle, age, and pigmentation. *Vision Research* 30, 5 (1990), 699–707.
- [18] MELLERIO, J., AND PALMER, D. A. Entopic halos and glare. *Vision Research* 12 (1972), 141–143.
- [19] MEYER, G. W. Wavelength selection for synthetic image generation. *Computer Vision, Graphics, and Image Processing* 41 (1988), 57–79.
- [20] NAKAMAE, E., KANEDA, K., OKAMOTO, T., AND NISHITA, T. A lighting model aiming at drive simulators. *Computer Graphics* 24, 3 (August 1990), 395–404. ACM Siggraph '90 Conference Proceedings.
- [21] ORDY, J. M., BRIZZEE, K. R., AND JOHNSON, H. A. Cellular alterations in visual pathways and the limbic system: Implications for vision and short-term memory. In *Aging and Human Visual Function*, R. Sekular, D. Kline, and K. Dismukes, Eds., vol. 2 of *Modern Aging Research*. Alan R. Liss, Inc., 1982, pp. 79–114.
- [22] OWSLEY, C., SEKULER, R., AND SIEMSEN, D. Contrast sensitivity throughout adulthood. *Vision Research* 23, 7 (1983), 689–699.
- [23] REA, M. S., Ed. *The Illumination Engineering Society Lighting Handbook*, 8th ed. Illumination Engineering Society, New York, NY, 1993.
- [24] RONCI, C., AND STEFANACCI, S. An annotated bibliography on some aspects of glare. *Att. Fond. Ronci* 30 (1975), 277–317.
- [25] ROSS, J. E., CLARKE, D. D., AND BRON, A. J. Effect of age on contrast sensitivity function: uniocular and binocular findings. *British Journal of Ophthalmology* 69 (1985), 51–56.
- [26] SAID, F., AND WEALE, R. The variation with age of the spectral transmissivity of the living human crystalline lens. *Gerontologia* 3, 4 (1959), 213.
- [27] SCHLICK, C. Quantization techniques for visualization of high dynamic range images. In *Proceedings of the Fifth Eurographics Workshop on Rendering* (June 1994), pp. 7–18.
- [28] SEKULER, R., AND BLAKE, R. *Perception*, second ed. McGraw-Hill, New York, 1990.
- [29] SIMPSON, G. Ocular halos and coronas. *British Journal of Ophthalmology* 37 (1953), 450–486.
- [30] SMITH, G., VINGRYS, A. J., MADDOCKS, J. D., AND HELY, C. P. Color recognition and discrimination under full-moon light. *Applied Optics* 33, 21 (1994), 4741–4748.
- [31] STILES, W. The effect of glare on the brightness difference threshold. *Proceedings of the Royal Society of London* 104 (1929), 322–351.
- [32] TUMBLIN, J., AND RUSHMEIER, H. Tone reproduction for realistic computer generated images. *IEEE Computer Graphics & Applications* 13, 7 (1993).
- [33] VOS, J. Disability glare- a state of the art report. *C.I.E. Journal* 3, 2 (1984), 39–53.
- [34] WARD, G. A contrast-based scalefactor for luminance display. In *Graphics Gems IV*, P. Heckbert, Ed. Academic Press, Boston, 1994, pp. 415–421.
- [35] WARD, G. J. The radiance lighting simulation and rendering system. *Computer Graphics* 28, 2 (July 1994), 459–472. ACM Siggraph '94 Conference Proceedings.
- [36] WYSZECKI, G., AND STILES, W. *Color Science: Concepts and Methods, Quantitative Data and Formulae*, second ed. Wiley, New York, N.Y., 1992.